Interference modeling and mitigation for GNSS receivers

Alexandre Brochard, Jessica Forner, Julien Goethal, Tristan Passeron, Lorenzo Ortega

Toulouse site

Interference modeling and mitigation for GNSS receivers

BROCHARD Alexandre / FORNER Jessica / GOETHAL Julien / PASSERON Tristan
Promo: *Aéro 5*
Class: *5TS1*

Course: *PMI* – Professor: *M. ORTEGA*
Submission date: *February 19, 2024*

Contents

Introduction

Context

Global Navigation Satellite Systems (GNSS) have revolutionized various industries by providing essential navigation, timing, and positioning information. Widely employed in applications ranging from intelligent transportation systems to autonomous unmanned vehicles, GNSS has become integral for critical operations. However, the original design of GNSS, tailored for clear sky nominal conditions, faces challenges in harsh environments, impacting performance and reliability. Notably, issues like multipath effects, reflections, spoofing, and intentional or unintentional interferences pose significant threats, especially in safety-critical scenarios such as civilian aviation.

Addressing these challenges requires robust interference mitigation strategies. State-of-the-art literature identifies various methods, among which pulse blanking, adaptive notch filtering and Karhunen-Loeve Transform (KLT) play pivotal roles. In this project, the focus is on countering interferences characterized by a constant envelope (CE), a significant family of intentional interferences, including pure and time-varying tones like chirped signals. These interferences exhibit a constant modulus property, leading to complex circular search spaces at the receiver.

The primary objectives of this project are threefold. Firstly, the exploration of existing methods proposed in the literature to mitigate constant envelope interferences. Secondly, the modeling and implementation of the interferences. Finally, the implementation and evaluation of selected interference mitigation methods.

To assess the performance of these mitigation strategies, the project adopts the Maximum Likelihood Estimator (MLE) for time-delay and Doppler shift estimation, comparing it post-countermeasure application. Further evaluation involves a comparison of mean square error (MSE) solutions with the theoretical limits given by the Cramér-Rao bound (CRB) under well-specified and misspecified conditional signal models, also known as misspecified Cramér-Rao bound (MCRB).

Matlab is chosen as the platform for project implementation due to its extensive library of base functions, facilitating signal and interference modeling as well as performance analysis.

At the project's conclusion, two deliverables will be provided: the Matlab source code for implementing interference mitigation methods and signal modeling and a comprehensive report discussing state-of-the-art algorithms, implementation details, obtained results, and future recommendations.

This project offers a unique learning opportunity, covering concepts of interference in aeronautical communication systems, its implications in electronic warfare, standard methods for attenuation, and the modeling and implementation of classic interference methods.

Motivations

Working as a group on the constant envelope interference mitigation project for GNSS provides a compelling opportunity for several reasons:

1. **Real-world Impact:** Our collaborative efforts directly impact the reliability of GNSS across critical applications, aligning with practical industry needs.

2. **Diverse Skill Sets:** Leveraging diverse backgrounds in electrical engineering, computer science, and signal processing, we enhance our collective expertise and tackle the project's interdisciplinary challenges.

3. **Efficient Division of Tasks:** Collaborating allows us to efficiently divide responsibilities based on individual strengths, ensuring comprehensive coverage of the project's scope.

4. **Innovation through Collaboration:** Working as a team fosters creative thinking, encouraging diverse perspectives that can lead to innovative solutions for interference mitigation.

5. **Professional Growth:** Group collaboration not only advances academic knowledge but also hones project management and communication skills, contributing to our overall professional development.

   Many in our group aspire to pursue careers in signal processing and GNSS technology. This collaborative project serves as a valuable opportunity for professional development, allowing us to gain practical insights and hands-on experience in a field we aim to join.

   Beyond academic benefits, active participation in this project provides exposure to the latest advancements, expands professional networks, and positions us at the forefront of industry trends. This endeavor is not just an academic exercise but a strategic investment in our collective professional growth.

   In essence, our motivation extends beyond academic curiosity; it is a proactive step towards shaping our future careers in signal processing and GNSS technology. Through collaborative learning and problem-solving, we aim to meet project objectives while laying the groundwork for ongoing success in our chosen professional paths.

Together, our motivation lies in addressing a significant challenge in GNSS technology, making meaningful contributions, and preparing for future collaborative and professional endeavors.

1 Concepts and Tools

1.1 Introduction

1.1.1 Context

Interference modeling and mitigation play crucial roles in enhancing the performance of GNSS receivers, such as GPS or Galileo. Interference can arise from various sources, including radio frequency signals, atmospheric conditions, or electronic devices. To address these challenges, interference modeling techniques are employed to analyze and understand the impact of different interference sources on GNSS signals. This idea is to implement at the receiver algorithms to distinguish between the GNSS signals broadcasting by the satellites and unwanted or intentional interference. Then, the receiver is required to mitigate the interference, enabling the position velocity and time (PVT) computation. Mitigation strategies involve the development of robust filtering algorithms, adaptive signal processing techniques, and advanced antenna designs to suppress interference effects. Additionally, the integration of multiple constellations and signal frequencies can enhance resilience against interference, ensuring reliable and accurate navigation solutions in challenging environments. As GNSS technology continues to evolve, ongoing research in interference modeling and mitigation remains crucial for achieving optimal performance in diverse real-world scenarios.

1.1.2 Estimation Theory

In general, GNSS signal reception and interference mitigation can be considered as a signal processing application. The received signal in our case have different properties :

- It's a random process due to environment noise (thermal noise for example).
- Every unknown parameter is stored in a vector $\boldsymbol{\theta}$.
- It can be sampled, so that a signal can always be represented as a vector of numbers.

Estimation problem can be expressed like this : $x = [x(1), ..., x(N)]^T$ is a vector of observations whose Probability Density Function (PDF), is written as $p(\boldsymbol{x}; \boldsymbol{\theta})$ is parameterized by a vector of unknown parameters : $\boldsymbol{\theta} = [\theta_1, ..., \theta_L]^T$ and those unknown parameters are the ones we want to estimate.

For that we will use what we called an estimator $\hat{\boldsymbol{\theta}}$ which is a function of the observations vector that we've seen previously : $\hat{\boldsymbol{\theta}} = \boldsymbol{g}(\boldsymbol{x})$

1.2 Background on deterministic estimation theory

1.2.1 Conditional Signal Model

A Conditional Signal Model (CSM) pertains to a model where the parameter of interest are assumed to be non-random, with the vector of unknown parameters $\boldsymbol{\theta}$ considered deterministic. In contrast, the Unconditional Signal Model (USM) describes a model in which the signal of interest is assumed to be random, with $\boldsymbol{\theta}$ having a prior distribution

that must be considered [1].

Let us consider the following CSM:

$$\boxed{\mathbf{x} = \mathbf{A}(\boldsymbol{\theta})\alpha + \mathbf{n}}$$

Where $\boldsymbol{A(\theta)} = [\boldsymbol{a}(\theta_1), ..., \boldsymbol{a}(\theta_L)]$ is the matrix of the measured signals $\boldsymbol{a}$ that depends on the components of the unknown parameters $\boldsymbol{\theta}, \boldsymbol{\alpha}^T = (\alpha_1, ..., \alpha_L)$ is the vector of real or complex amplitudes of the observed signals. Finally, $\mathbf{n}$ is the noise vector. It is often assumed to be an additive complex circular white Gaussian noise vector with unknown variance σ_n^2 so that : $\mathbf{n} \sim \mathcal{CN}(\mathbf{0}, \sigma_n^2 \mathbf{I}_N)$. Consequently the observed data PDF is also Gaussian with $\mathbf{x} \sim \mathcal{CN}(\mathbf{A}(\boldsymbol{\theta})\boldsymbol{\alpha}, \sigma_n^2 \mathbf{I}_N)$ and:

$$\boxed{p(\mathbf{x}; \theta) = \frac{1}{(\pi\sigma_n^2)^N} e^{-\frac{1}{\sigma_n^2}||\mathbf{x}-\mathbf{A}(\boldsymbol{\theta})\alpha||^2}} \tag{1}$$

The CSM described in (1) fits a large number of applications such as radar, sonar [2] or navigation. This is the signal model that we will consider for our case study, as has been done in numerous publications for the GNSS receiver under different conditions [3, 4, 5, 6, 7, 8, 9, 10, 11].

1.2.2 Estimator Quality

Considering the CSM along with its PDF, the vector that contains all the unknown parameters can be defined as $\boldsymbol{\epsilon}^T = (\sigma_n^2, \boldsymbol{\theta}^T, \boldsymbol{\alpha}^T)$. So $\hat{\boldsymbol{\epsilon}}$ is an estimator of $\boldsymbol{\epsilon}$. An estimator fulfill these requirements:

- An estimator is a random variable. It is a function of the data and is consequently a function of random variables with its own properties.
- The bias of an estimator is a statistical measure that indicates how the expected value of the estimator consistently deviates from the true parameter to estimate. One can determine the bias of the estimator by:

$$\boxed{\boldsymbol{b}(\hat{\boldsymbol{\epsilon}}) \triangleq E\{\hat{\boldsymbol{\epsilon}}\} - \boldsymbol{\epsilon}}$$

  where $E\{\}$ is the expectation operator.

- The variance of an estimator is a statistical metric that measures the spread of the estimator's values around its expected value (mean).

$$\boxed{\mathrm{Var}(\hat{\epsilon}) \triangleq E\left\{(\hat{\epsilon} - E\{\hat{\epsilon}\})^2\right\}}$$

For vectors, one refers to the covariance matrix:

$$\boxed{\mathbf{C}_{\hat{\boldsymbol{\epsilon}}} \triangleq E\left\{(\hat{\boldsymbol{\epsilon}} - E\{\hat{\boldsymbol{\epsilon}}\})(\hat{\boldsymbol{\epsilon}} - E\{\hat{\boldsymbol{\epsilon}}\})^T\right\}}$$

The smaller this variance or covariance matrix is, the better the estimation is in terms of precision.

- Another metric that includes both bias and variance is the Mean Squared Error (MSE) defined as:

$$\boxed{\text{MSE}(\epsilon_i) \triangleq E\left\{(\hat{\epsilon}_i - \epsilon_i)^2\right\} = \mathbf{b}(\hat{\epsilon}_i)^2 + \text{var}(\hat{\epsilon}_i), \text{ for } i \in [1, L].}$$

For unbiased estimators, variance and MSE are the same.

Now let $\boldsymbol{\epsilon}_N$ be an estimator of $\boldsymbol{\epsilon}$ based on N signal samples. $\boldsymbol{\epsilon}_N$ is a wide sense consistent estimator if it converges in probability :

$$\boxed{\lim_{N \to +\infty} P[||\hat{\boldsymbol{\epsilon}}_N - \boldsymbol{\epsilon}|| < \delta] = 1, \ \forall \delta > 0, \ \forall \boldsymbol{\epsilon}}$$

where $P[event]$ denotes the probability of event. Similarly, $\hat{\boldsymbol{\epsilon}}_N$ is consistent in mean square if:

$$\boxed{\lim_{N \to +\infty} E\left\{(\widehat{\boldsymbol{\epsilon}}_N - \boldsymbol{\epsilon})(\widehat{\boldsymbol{\epsilon}}_N - \boldsymbol{\epsilon})^T\right\} = 0, \forall \boldsymbol{\epsilon}}$$

and if an estimator is consistent in mean square, it is wide sense consistent as well. Typically, users tend to prioritize mean square consistency as it is more manageable for proofs. The remaining concern revolves around the convergence speed, which can vary among different estimators. An ideal estimator would be one that is not only consistent but also exhibits rapid convergence, indicating minimal variance. The Cramér-Rao bound (CRB) is a tool that establishes a minimum limit for the variance of any locally unbiased estimator. This lower bound plays a crucial role in comparing various estimators and assessing the potential for improvement in an estimator. An estimator is considered efficient if it is unbiased and its variance matches the corresponding CRB.

The CRB is defined for cases where the PDF $p(\boldsymbol{x}; \boldsymbol{\epsilon})$ fits the following regularity condition:

$$\boxed{E\left\{\frac{\partial \ln p(\mathbf{x}; \boldsymbol{\epsilon})}{\partial \boldsymbol{\epsilon}}\right\} = 0\,, \ \forall \boldsymbol{\epsilon}.}$$

Then, for any unbiased estimator $\hat{\boldsymbol{\epsilon}}$, its covariance matrix $\boldsymbol{C}_{\hat{\boldsymbol{\epsilon}}}$ satisfies

$$\boxed{\mathbf{C}_{\hat{\boldsymbol{\epsilon}}} - \mathbf{F}^{-1}_{\boldsymbol{\epsilon}|\boldsymbol{\epsilon}}(\boldsymbol{\epsilon}) \geq 0\,,}$$

where $\mathbf{F}_{\boldsymbol{\epsilon}|\boldsymbol{\epsilon}}$ is the Fisher Information Matrix (FIM) defined as:

$$\boxed{\mathbf{F}_{\boldsymbol{\epsilon}|\boldsymbol{\epsilon}}(\boldsymbol{\epsilon}) = -E\left\{\frac{\partial^2 \ln p(\mathbf{x}; \boldsymbol{\epsilon})}{\partial \boldsymbol{\epsilon} \partial \boldsymbol{\epsilon}^T}\right\}}$$

and the second derivative is evaluated at the true value of $\boldsymbol{\epsilon}$. At the GNSS receiver, the signal at the output of the Hilbert filter can can be modeled as a complex circular Gaussian distribution: $\mathbf{x} \sim \mathcal{CN}(\boldsymbol{\mu}(\boldsymbol{\epsilon}), \mathrm{C}(\boldsymbol{\epsilon}))$ where $\mu(\epsilon)$ is the mean vector, which represent the baseband signal time-delayed and $\mathrm{C}(\boldsymbol{\epsilon})$ is the covariance matrix. For this particular case, the Slepian-Bangs formulas give an expression of the FIM [12]:

$$\boxed{\left[\mathrm{F}_{\boldsymbol{\epsilon}|\boldsymbol{\epsilon}}(\boldsymbol{\epsilon})\right]_{k,l} = 2\mathrm{Re}\left\{\frac{\partial \mu^H(\boldsymbol{\epsilon})}{\partial \boldsymbol{\epsilon}_k}\mathrm{C}(\boldsymbol{\epsilon})^{-1}\frac{\partial \mu(\boldsymbol{\epsilon})}{\partial \boldsymbol{\epsilon}_l}\right\} + \mathrm{Tr}\left\{\mathrm{C}(\boldsymbol{\epsilon})^{-1}\frac{\partial \mathrm{C}(\boldsymbol{\epsilon})}{\partial \boldsymbol{\epsilon}_k}\mathrm{C}(\boldsymbol{\epsilon})^{-1}\frac{\partial \mathrm{C}(\boldsymbol{\epsilon})}{\partial \boldsymbol{\epsilon}_l}\right\}}$$

where $Tr\{\cdot\}$ represents the trace operator. It is worth mentioning that in the context of GNSS, the parameters to be estimated are those contained within the mean vector. Recently, closed-form CRBs expressions [3, 13, 14, 15, 16, 17] for the associated parameter of interest have been derived under specific assumptions, which will be elaborated on later in the document. Furthermore, numerous publications have utilized these expressions and confirmed their effectiveness.

Having acquired knowledge about standard tools for characterizing an estimator, the objective is now to construct an estimator that is as effective as possible, preferably an efficient one. However, achieving this is not always feasible, and the subsequent section is dedicated to defining a set of estimators grounded in the maximum likelihood principle.

1.2.3 Maximum Likelihood Estimator

Finding a highly effective estimator for a particular problem is not always feasible. In signal processing, a commonly adopted approach is to resort to the Maximum Likelihood Estimator (MLE) [18], which exhibits numerous asymptotic properties, making it a relevant option. The MLE principle is simply to find the parameter $\boldsymbol{\epsilon}$ that maximizes the likelihood function $p(\boldsymbol{x};\boldsymbol{\epsilon})$, which is the PDF when $\boldsymbol{x}$ is fixed and equal to the observed data:

$$\boxed{\widehat{\boldsymbol{\theta}} = \arg\max_{\boldsymbol{\epsilon}} p(\mathbf{x};\boldsymbol{\epsilon})}$$

The MLE possesses a noteworthy characteristic: it is asymptotically efficient. In other words, as the number of observations increases or as the signal-to-noise ratio (as defined later) grows large, the MLE becomes unbiased, and its variance equals the CRB. The MLE seeks the vector $\boldsymbol{\epsilon}$ that maximizes the likelihood. There is often a temptation to examine the log-likelihood in order to eliminate the exponential term.

$$\boxed{\hat{\boldsymbol{\epsilon}} = \arg\max_{\boldsymbol{\epsilon}}\left\{\ln p(\mathbf{x};\boldsymbol{\epsilon})\right\} = \arg\max_{\boldsymbol{\epsilon}}\left\{-N\ln(\pi) - N\ln\left(\sigma_n^2\right) - \frac{1}{\sigma_n^2}\left\|\mathbf{x} - \mathbf{A}(\boldsymbol{\theta})\boldsymbol{\alpha}\right\|^2\right\}.}$$

For the estimation of the variance term, σ_n^2, one can find the σ_n^2 that cancels the first derivative of the log-likelihood.

$$\boxed{\frac{\partial \ln p(\mathbf{x};\boldsymbol{\theta})}{\partial \sigma_n^2} = -\frac{N}{\sigma_n^2} + \frac{1}{\sigma_n^4}||\mathbf{x} - \mathbf{A}(\boldsymbol{\theta})\alpha||^2,}$$

so that that maximum likelihood estimate of the noise variance is simply:

$$\boxed{\widehat{\sigma_n^2} = \frac{1}{N}||\mathbf{x} - \mathbf{A}(\boldsymbol{\theta})\boldsymbol{\alpha}||^2.}$$

By replacing this estimate in the log-likelihood and omitting the constant terms, the MLE problem becomes:

$$\boxed{\left(\hat{\boldsymbol{\theta}}, \hat{\alpha}\right) = \arg\max_{\boldsymbol{\theta},\alpha} \left\{-\ln\left(\|\mathbf{x} - \mathbf{A}(\boldsymbol{\theta})\alpha\|^2\right)\right\} = \arg\min_{\epsilon} \left\{\|\mathbf{x} - \mathbf{A}(\boldsymbol{\theta})\boldsymbol{\alpha}\|^2\right\}.}$$

Let $\mathbf{P_A} = \mathbf{A}(\boldsymbol{\theta})\left(\mathbf{A}(\boldsymbol{\theta})^H\mathbf{A}(\boldsymbol{\theta})\right)^{-1}\mathbf{A}(\boldsymbol{\theta})^H$ be the orthogonal projector on the vector space defined by the column of $\mathbf{A}(\boldsymbol{\theta})$, also referred as the data vector space. Then $\mathbf{P}_{\mathrm{A}}^{\perp} = \mathbf{I} - \mathbf{P}_{\mathrm{A}}$ is the orthogonal projector on the noise space, and one can decompose the norm to be minimized as follows:

$$\boxed{||\mathbf{x} - \mathbf{A}(\boldsymbol{\theta})\boldsymbol{\alpha}||^2 = \left\|\left(\mathbf{P}_{\mathrm{A}} + \mathbf{P}_{\mathrm{A}}^{\perp}\right)(\mathbf{x} - \mathbf{A}(\boldsymbol{\theta})\boldsymbol{\alpha}\right\|^2 = \|\mathbf{P}_{\mathrm{A}}(\mathbf{x} - \mathbf{A}(\boldsymbol{\theta})\boldsymbol{\alpha})\|^2 + \left\|\mathbf{P}_{\mathrm{A}}^{\perp}(\mathbf{x} - \mathbf{A}(\boldsymbol{\theta})\boldsymbol{\alpha})\right\|^2}$$

and resorting to the definition of the projectors, one gets :

$$\boxed{||\mathbf{x} - \mathbf{A}(\boldsymbol{\theta})\boldsymbol{\alpha}||^2 = \left\|\mathbf{A}\left(\left(\mathbf{A}(\boldsymbol{\theta})^H\mathbf{A}(\boldsymbol{\theta})\right)^{-1}\mathbf{A}(\boldsymbol{\theta})^H - \boldsymbol{\alpha}\right)\right\|^2 + \left\|\mathbf{P}_{\mathbf{A}}^{\perp}\mathbf{x}\right\|^2.}$$

The goal is to minimize both terms of the previous equation. The first term minimization yields a closed-form for the estimation of the complex amplitude:

$$\boxed{\hat{\boldsymbol{\alpha}} = \mathbf{A}(\boldsymbol{\theta})^H\mathbf{A}(\boldsymbol{\theta}))^{-1}\mathbf{A}(\boldsymbol{\theta})^H}$$

and the minimization problem reduces to:

$$\boxed{\hat{\boldsymbol{\theta}} = \arg\min \boldsymbol{\theta}\left\{||\mathbf{P}_{\mathbf{A}}^{\perp}\mathbf{x}||^2\right\} = \arg\max \boldsymbol{\theta}\left\{||\mathbf{P}_{\mathbf{A}}\mathbf{x}||^2\right\}}$$

The MLE becomes a robust estimator due to its asymptotic properties. However, its effectiveness depends on the signal model and the complexity of parameter estimation. In some cases, particularly when dealing with a multidimensional signal model and many parameters, the MLE can pose challenges as it transforms into a highly non-linear optimization problem. This complexity can render it intractable, primarily due to the associated computational costs. Alternative methods are available to address the complexity of the MLE. In various scenarios, such as in an array of sensors, sophisticated algorithms, such as the Multiple Signal Classification (MUSIC) [19] and the Capon algorithm [20],

have been extensively researched for decades and continue to serve as benchmarks in the field.

1.2.4 Misspecified Estimation

Until now, the estimation problem assumed a thorough understanding of the signal model under examination. With this understanding, the PDF of the data could be formulated, the corresponding CRB assessed, and the MLE, or at least suboptimal versions of it, could be implemented. However, the signal model is not always well-established. Alternatively, the true model might result in estimators that are too complex. One approach to address this challenge is to assume a simplified signal model. When the assumed model differs from the true data model, it is considered misspecified [21, 22, 23, 24]. Such misspecification can impact overall estimation performance in terms of bias and variance. This case perfectly describes the case of low-cost receivers, which do not implement interference mitigation measures. In this case, the receiver assumes an interference-free reception model, however the reality differs, as interference is part of the true signal model.

Let $p(\boldsymbol{x})$ be the PDF of the true data signal model and $f(\boldsymbol{x};\boldsymbol{\theta})$ be the PDF of the assumed data signal model. If one applies the misspecified MLE (MMLE), that is, the MLE that corresponds to the assumed signal model, to the observed data x, in the limit of large sample support or at high SNR for the CSM, the estimated $\hat{\boldsymbol{\theta}}$ converges to the vector $\boldsymbol{\theta}_{pt}$, also known pseudo-parameter vector, and which would be the one that minimizes the Kullback-Leibler Divergence (KLD) between the PDF of the true and the assumed signal model.

$$\boxed{\boldsymbol{\theta}_{pt} = \arg\min_{\theta} \{D\left(p_{\bar{x}} \| f_{\bar{x}}\right\} = \arg\min_{\theta} \{E_p\left\{\ln p(\mathbf{x}) - \ln f(\mathbf{x};\theta)\right\}\}}$$

The pseudotrue-parameter might vary significantly from the expected value depending on the degree of misspecification of the considered scenario. Furthermore, as mentioned earlier, the MMLE is asymptotically consistent and the corresponding variance is equal to a lower bound provided by the so-called Misspecified CRB (MCRB) [25]. In other words, the MMLE is an efficient estimator of this pseudo-true parameter and the MCRB is a generalization of the CRB defined by the following equation:

$$\boxed{\mathrm{MCRB}(\boldsymbol{\theta}_{pt}) = \mathrm{A}(\boldsymbol{\theta}_{pt})^{-1}\mathrm{B}(\boldsymbol{\theta}_{pt})\mathrm{A}(\boldsymbol{\theta}_{pt})^{-1}}$$

where

$$\boxed{[\mathbf{A}(\boldsymbol{\theta}_{pt})]_{k,l} = E_p\left\{\left.\frac{\partial^2 \ln f(\mathbf{x};\boldsymbol{\theta})}{\partial\theta_k \partial\theta_l}\right|_{\boldsymbol{\theta}=\boldsymbol{\theta}_{pt}}\right\},}$$

and

$$\boxed{[B(\boldsymbol{\theta}_{pt})]_{k,l} = E_p\left\{\left.\frac{\partial \ln f(\mathbf{x};\boldsymbol{\theta})}{\partial\theta_k}\right|_{\boldsymbol{\theta}=\boldsymbol{\theta}_{pt}} \cdot \left.\frac{\partial \ln f(\mathbf{x};\boldsymbol{\theta})}{\partial\theta_l}\right|_{\boldsymbol{\theta}=\boldsymbol{\theta}_{pt}}\right\}.}$$

These expressions highly depend on the model misspecification. Depending on the

scenario, they can be further developed to obtain nicer forms.

This section enables the characterization of misspecified estimators when the data model is unknown and avoiding misspecification is not possible. It is worth mentioning that significant contributions have been made in the field of GNSS misspecification theory. Specifically, research has been conducted on the degradation resulting from not accounting for multipath scenarios. To address this, pseudo-parameters have been derived, and closed-form expressions of the Pseudo-parameters and MCRB have been obtained [26, 27, 28]. Additionally, the estimation performance of parameters in high dynamic scenarios, involving the presence of acceleration parameters, has been assessed. Once again, pseudo-parameters were computed, and closed expressions of the MCRB were derived [29]. Furthermore, there have been contributions regarding scenarios where interferences degrade receiver performance. In these cases, pseudo-parameters were calculated for various scenarios [30, 31], and MCRBs were derived for different types of interference [32].

1.3 Global Navigation Satellite Systems

Navigation encompasses the art and science of monitoring and directing the movement of objects from one point to another, whether it's an individual trekking in the mountains using traditional tools like a paper map, compass, and landmarks or a vehicle on Earth requiring knowledge of its position, velocity, and orientation. One prominent category within navigation solutions leverages radio frequency (RF) signals and is termed radionavigation.

In the late 1970s, the United States launched the inaugural Navigation System with Timing and Ranging (NAVSTAR) satellite, marking the genesis of the Global Positioning System (GPS). Originally designed to provide precise estimates of an object's position, velocity, and attitude worldwide, GPS set the stage for a new era in navigation technology. Subsequently, various countries developed their own navigation satellite systems, including the Russian Federation's Global Navigation Satellite System (GLONASS), China's BeiDou system, the European GALILEO system, India's Navigation with Indian Constellation (NavIC), and Japan's Quasi-Zenith Satellite System (QZSS). The amalgamation of these systems, along with their enhancements, constitutes what is widely recognized as the Global Navigation Satellite Systems (GNSS).

This network of satellites collaboratively facilitates accurate and widespread positioning, navigation, and timing information, making GNSS an indispensable tool in a multitude of applications ranging from civilian navigation to scientific research and military operations. As we delve into the intricacies of GNSS in the following sections, we aim to unravel its principles, constellations, and signal structures, laying the foundation for a comprehensive understanding of interference modeling and mitigation for GNSS receivers.

1.3.1 Principle

GNSS operate on the fundamental principle of trilateration, utilizing constellations of Medium Earth Orbit (MEO) satellites or Space Vehicles (SV) distributed across three or six orbital planes. This configuration ensures that users worldwide have visibility to a minimum of four to eight satellites at any given time, regardless of their location on Earth's surface.

Each satellite within the constellation continuously transmits a known ranging signal towards Earth. A GNSS receiver captures and identifies the signal, determining which

SV transmitted it. Moreover, the receiver calculates the time (τ) elapsed between the signal transmission and reception. The product of this time, τ, and the speed of light (c) provides a measure of the radio-electric distance between the SV and the receiver.

By performing this range estimation with signals from at least three satellites and knowing the positions of all SVs, the receiver can compute its own position through trilateration. This foundational concept of GNSS is illustrated in Figure 1.

To refine the position estimate and obtain a more accurate solution, a fourth measurement is incorporated to address receiver clock uncertainty. Receiver clocks typically employ standard quality oscillators that require continuous estimation, while SVs are equipped with highly stable and precise atomic clocks. The process of solving the trilateration problem, considering the Doppler effect, time, and additional measurements, is commonly known as obtaining a Position-Velocity-Time (PVT) solution. This principle forms the bedrock of GNSS functionality, enabling a myriad of applications ranging from navigation in daily life to advanced scientific and military operations.

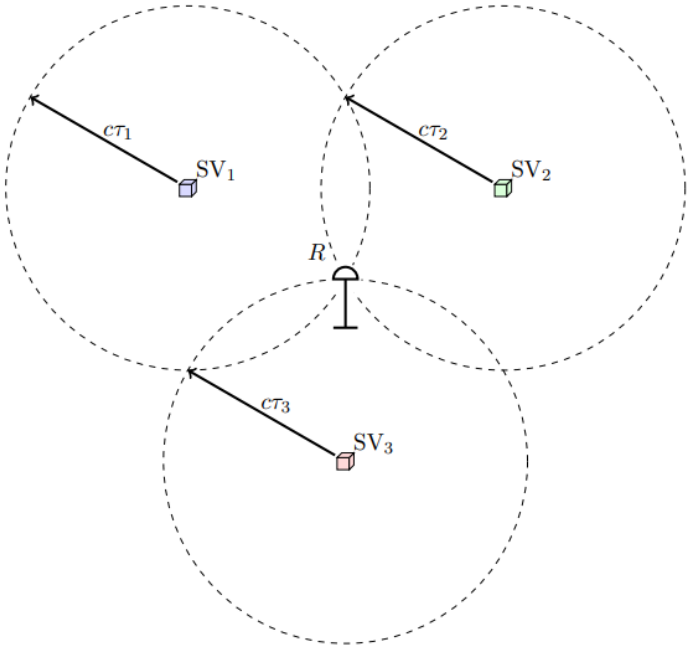

Figure 1: Schematic representation of a pulse blanker

1.3.2 Constellations & Signals

General GNSS Signal Structure

The challenge in designing Global Navigation Satellite System (GNSS) signals lies in creating a signal family that not only facilitates detection but also enables the identification of the corresponding transmitting Space Vehicle (SV). Moreover, the chosen signal must ensure high-ranging precision for an accurate solution to the Position-Velocity-Time (PVT) problem. To meet these requirements, GNSS signals employ a spreading technique known as Direct Sequence Spread Spectrum (DSSS).

This spreading technique involves multiplying a low data rate signal with a high data rate Pseudo-Random Noise (PRN) sequence. Removal of the spreading is achieved

through cross-correlation with the correct PRN sequence upon signal reception. The selection of the PRN sequence must adhere to specific properties. Firstly, the auto-correlation function (ACF) of a sequence should exhibit a main peak significantly higher than others, ideally with sharpness for optimal estimation performance. Secondly, the cross-correlation function (CCF) between two different sequences, corresponding to different SVs within the same constellation, should feature very low values, ensuring quasi-orthogonality between PRN codes.

For modernized signals, only the data channel carries a navigation message. It's important to note that for signals of the BOC family, an additional feature, the subcarrier ($sc(t)$), is part of the signal definition, tuning spectral occupancy and signal ranging performance.

All GNSS signals considered here can be described by three primary elements:

- **Carrier frequency (f_c):** Denotes the center frequency of the transmitted signal.
- **Ranging code or PRN sequence ($c(t)$):** A family of codes that should be quasi-orthogonal, with each code comprising N_c discrete values of duration T_c called chips. Ranging codes are often transmitted at a high rate, e.g., $F_0 = 1023000$ Hz or multiples of F_0.
- **Navigation message ($d(t)$):** Contains all necessary data to compute the position of the transmitting satellite, a prerequisite for obtaining a PVT solution. This coded message is transmitted on GNSS data channels at a slower rate (e.g., 50 Hz for GPS L1 C/A).

The transmitted signal is then a product of all these components, modulated at frequency f_c:

$$s_T = d(t)c(t)\cos(2\pi f_c t) \tag{2}$$

Global Positioning System (GPS)

The NAVSTAR GPS [33] space segment comprises 24 or more satellites evenly distributed across 6 quasi-circular orbital planes, each inclined at 55 degrees. This configuration ensures that four or more satellites are continually visible from any point on Earth, facilitating the computation of a Position-Velocity-Time (PVT) solution at any location. The satellites orbit at an average altitude of 20,200 km, with a revolution period of half a sidereal day. Consequently, considering the Earth's rotation, the satellite ground tracks are revisited every sidereal day.

GPS broadcasts several signals across three bands: L1 with a carrier frequency $f_{L1} = 1575.42$ MHz, L2 with $f_{L2} = 1227.60$ MHz, and L5 with $f_{L5} = 1176.45$ MHz. Initially, signals over L1 were modulated by the Coarse Acquisition (C/A) code and the Precise (Encrypted) (P(Y)) code. The C/A code, designed for civil open-access use, is the most widely utilized. It consists of a low-rate navigation message (50 bits per second) spread with a PRN code from the Gold family with a length of $N_c = 1023$. The PRN code is modulated using Binary Phase Shift Keying (BPSK) modulation at a clock rate of 1.023 MHz, denoted as BPSK(1), where the number in parentheses is a multiple of the frequency $f_0 = 1.023$ MHz. As a result, the code duration is 1 ms, and the main lobe of its Power Spectral Density (PSD) is 2.046 MHz wide.

Over time, the GPS system has undergone modernization, introducing blocks IIR(M), IIF, and more recently, blocks III satellites transmitting military M code, L1C, L2C, and L5 codes with distinct time and spectral properties. For instance, the L5 signal possesses the unique feature of being separated into two orthogonal channels: the in-phase channel with BPSK(10) modulation carrying the navigation message (data channel), and the quadrature channel, also employing BPSK(10) modulation but without a navigation message (pilot channel). Pilot channels are designed for extended integration processing.

Galileo

The GALILEO program [34] stands as a European initiative to develop and operate an independent Global Navigation Satellite System (GNSS). The GALILEO space segment consists of 30 Medium Earth Orbit (MEO) satellites evenly distributed across three quasi-circular orbital planes with a 56-degree inclination and an average altitude of 23,222 km. Each satellite takes 14 hours to complete an orbit around the Earth, resulting in a ground track revisiting time of 7 sidereal days.

GALILEO signals are transmitted across three bands: $E1$ with a carrier frequency $f_{E1} = f_{L1}$, $E5$ with $f_{E5} = 1191.795$ MHz, and $E6$ with $f_{E6} = 1278.75$ MHz. Additionally, the $E5$ band can be seen as two side-by-side bands: $E5A$ with $f_{E5A} = f_{L5}$ and $E5B$ with $f_{E5B} = 1207.14$ MHz. Notably, the $E1$ and $E5A$ bands share the same carrier frequencies as GPS L1 and L5 bands, fostering interoperability between the two constellations. A GPS receiver would only require an update at the processing stage, not the RF front-end, to function as a GALILEO receiver.

For GALILEO $E1$ Open Service (OS) signals, which are the most common, two channels are transmitted simultaneously: i) the data stream $E1B$ and ii) the pilot stream $E1C$. Both components have a spreading code with 4092 chips over 4 ms and are modulated by a Composite Binary Offset Carrier (CBOC(6,1)) modulation. $CBOC$ is defined as a combination of two Binary Offset Carrier (BOC) modulations, specifically a $BOC(1,1)$ and a $BOC(6,1)$. $BOC(m,n)$ serves as an alternative to BPSK pulse shaping, with parameters $fs = m \cdot f_0$ for sub-carrier frequency and $fc = n \cdot f_0$ for code chipping rate, producing different temporal and spectral properties based on the choices of n, m, and the cosine or sine function.

The $E5$ band has a unique structure, consisting of two side-by-side bands ($E5A$ and $E5B$). Both bands employ $BPSK(10)$ modulations with in-phase data channels and quadrature pilot channels. When combined, the resulting signals over the entire $E5$ band create a complex signal known as Alternative BOC or AltBOC, characterized by a broad bandwidth, facilitating potential high-accuracy measurements.

1.3.3 GNSS receivers : Signal Processing

Now that an overview of the main GNSS signals has been done, the question of how these signals are processed to obtain a final position must be addressed. In particular, in this section, the focus is done on the two very first steps of a standard GNSS signal processing, namely, the acquisition and the tracking stages whose outputs are the pseudo-ranges between the receiver and each satellites in view.

Considering the reception of four different satellite signals of the same constellation and assuming an ideal model (all clocks synchronized, no group delay at transmitters and receiver level, no group delay from ionosphere and troposphere, no relativistic effect), the

baseband signal, that is, after filtering, down-conversion and sampling, can be written as:

$$\mathbf{x} = \sum_{i=1}^{4} \alpha_i \mathbf{s}_i(\tau_i, F_{d,i}) + \mathbf{w}$$

where, $\mathbf{w}$ is a complex additive white Gaussian noise so that $\mathbf{w} \sim \mathcal{CN}(0, \sigma_n^2 \mathbf{I}_N)$ and for $n \in [1, N]$ the sample index,

$$\mathbf{x}^T = (\ldots, x(nTs), \ldots),$$
$$\mathbf{s}_i(\tau_i, F_{d,i})^T = (\ldots, s(nTs - \tau_i)e^{-j2\pi F_{d,i}(nTs-\tau_i)}, \ldots),$$
$$\mathbf{w}^T = (\ldots, w(nTs), \ldots),$$

Ts the sampling period, for $i \in [1, 4]$, α_i is the complex amplitude of the i-th signal, τ_i is the time-delay, and $F_{d,i}$ is the Doppler frequency. This model or its continuous-time version are typical models that are used in most of the GNSS literature.

For the considered CSM, the acquisition step aims to provide an estimate of $(\tau_i, F_{d,i})$ for each satellite in view. The classical approach is to compute the cross-correlation between the received signal and each satellite PRN code and take the set (τ, Fd) that maximizes this function. This is somehow equivalent to a single-source maximum likelihood estimator or 1S-MLE, as predicted in the interpretation of the MLE. This CCF, also known as ambiguity function, can be defined as:

$$R_{x,si}(\tau, Fd) = T\mathbf{s}_i(\tau, Fd)^H \mathbf{x} \tag{3}$$

Thanks to the quasi-orthogonality of the PRN sequences, if the signal of the i-th SV is in the received signal, the CCF will present a single peak that is located around the true values of (τ_i, Fd_i). Otherwise, the CCF will present only small values that correspond to the noise floor. This has been illustrated in Figure 2

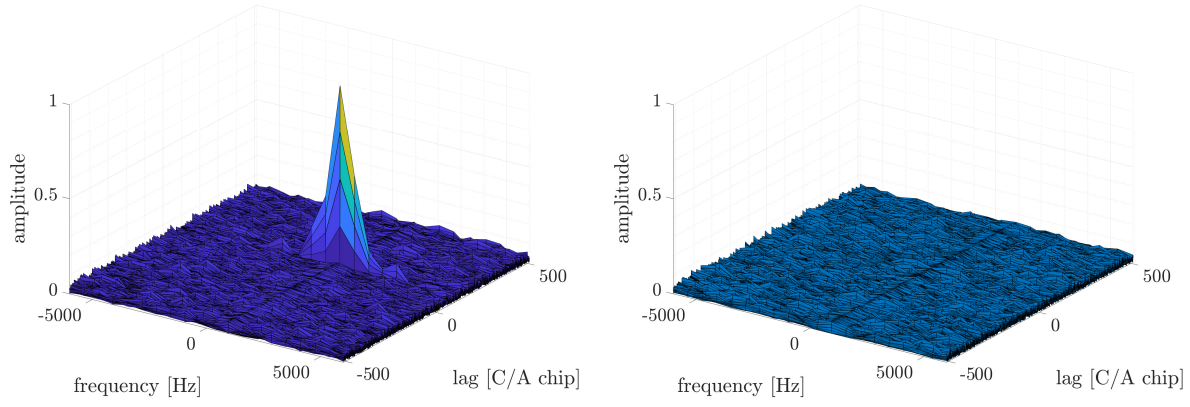

(a) (b)

Figure 2: Example of ambiguity function in two cases, (**a**) the PRN tested is present in the received signal and (**b**) the PRN tested is not present in the received signal [35].

In conclusion, our exploration of GNSS has covered the principles, constellations, and signal structures that drive this transformative technology. From the inception of GPS in the late 1970s to the collaborative efforts of various constellations, including GPS, GLONASS, GALILEO, BeiDou, NavIC, and QZSS, GNSS has become integral to positioning, navigation, and timing globally.

The trilateration principle, utilizing MEO satellites or SVs, is fundamental to GNSS functionality. We delved into signal intricacies, such as ranging codes and navigation messages, highlighting the design complexities of signals like GPS and GALILEO. Signal

processing, with a focus on acquisition and tracking, revealed the significance of cross-correlation functions in estimating time-delay and Doppler frequency.

1.4 How to model an Interference Signal at the GNSS receiver

In the realm of Global Navigation Satellite Systems (GNSS) signal processing, the interference mitigation process assumes a central role by alleviating the impact of various radiofrequency interference (RFI) sources and noise on received GNSS signals. Mitigation techniques are purposefully designed algorithms intended to counteract the adverse effects introduced by external factors, thereby ensuring the resilience and precision of GNSS receiver positioning and navigation capabilities.

To effectively tackle this challenge, the first step involves characterizing the interferences and having tools to assess their impact on the receiver. In the context of GNSS receivers, interferences can introduce biases in estimating synchronization parameters like time delay and Doppler frequency. In the past year, some tools to analyze the effects of interferences on GNSS receivers have been derived. These tools [32] are built upon the misspecified estimation theory discussed in Section 1.2.4. Our focus is primarily on the signal model, where the received signal at the output of the receiver's Hilbert filter can be approximated by.

$$x(t;\boldsymbol{\epsilon}) = \rho e^{j\Phi} s(t-\tau) e^{-j2\pi f_c b(t-\tau)} + I(t) + w(t;\sigma_n^2). \tag{4}$$

which differs from the signal model considered in reception, which does not assume the presence of interference:

$$x\left(t;\boldsymbol{\phi}\right) = \kappa(t;\boldsymbol{\theta}) + w(t;\sigma_n^2) \tag{5}$$

with

$$\kappa(t;\boldsymbol{\theta}) = \rho e^{j\Phi} s(t-\tau) e^{-j2\pi f_c b(t-\tau)}, \tag{6}$$

and $\boldsymbol{\epsilon}^\top = (\sigma_n^2, \rho, \Phi, \boldsymbol{\eta}^\top)$, where σ_n^2 is the power of the white noise vector $\mathbf{w}$ (such that $\mathbf{w} \sim \mathcal{CN}(\mathbf{0}, \sigma_w^2 \mathbf{I}_N)$). Note that $\boldsymbol{\eta}^\top = [\tau, b]$ and represents the time-delay and Doppler effect. Those parameters are the parameter of interest to be estimated. The primary goal of a mitigation techniques is to enhance signal quality by mitigating the effects of interference $I(t)$ at the GNSS receiver. In this project, our focus will be on intentional interference. Within this category, the most recognized interferences in the state-of-the-art include the following:

- **Pulse Gaussian interference** introduces random noise peaks in order to prevent the receiver from demodulating the navigation message. These noise peaks can be characterized by a Gaussian noise distribution with a variance of several orders of magnitude greater than the power of the thermal noise.
- **Tone interference** introduces a single tone located at a frequency f_i. The interference at the output of the receiver's Hilbert filter is defined as:

  $$I(t) = A_i e^{j2\pi f_i t + j\phi} \tag{7}$$

  where A_i denotes the amplitude of the tone and ϕ denotes the initial phase. These interferences are known to be the first identified in the state of the art. Due to the fact that GNSS signals are of higher bandwidth, their effects can be mitigated more easily.

- **Chirp interference** introduces a tone which change the instantaneous frequency with respect to the time. These interference can be both narrowband and broadband generating many more problems when implementing mitigation methods. The most commonly used chirp is linear frequency modulation (LFM) which at the output of the receiver's Hilbert filter can be modeled as:

$$I(t) = \Pi_T(t) \times e^{j\pi\alpha_c t^2 + j\phi},\ \Pi_T(t) = \begin{cases} A_i & \text{for } 0 \leq t < T \\ 0 & \text{otherwise} \end{cases}, \tag{8}$$

with α_c the chirp rate, A_i the amplitude and $T = NT_s$ the waveform period. The instantaneous frequency is $f(t) = \frac{1}{2\pi}\frac{d}{dt}(\pi\alpha_c t^2) = \alpha_c t$, and therefore the waveform bandwidth is $B = \alpha_c T$. We consider the case where, after the Hilbert filter, the chirp is located at the baseband frequency, i.e., the central frequency of the chirp is $f_i = 0$. Then, the chirp equation can be rewritten as,

$$I(t) = \Pi_T(t) \times e^{j\pi\alpha_c (t-T/2)^2 + j\phi},\ \Pi_T(t) = \begin{cases} A_i & \text{for } 0 \leq t < T \\ 0 & \text{otherwise} \end{cases}. \tag{9}$$

It should be noted that in the last few years definitions of non-linear frequency modulation chirps [36] have appeared. Those can be defined as:

$$I(t) = \Pi_T(t) \times e^{j\pi\varphi(\beta_c;t) + j\phi},\ \Pi_T(t) = \begin{cases} A_i & \text{for } 0 \leq t < T \\ 0 & \text{otherwise} \end{cases} \tag{10}$$

where $\varphi(\beta_c; t)$ is a non-linear function with β_c a parameter which controls the bandwidth of the chirp.

1.4.1 Mitigation Techniques

Mitigation techniques are characterized by their ability to selectively suppress or minimize the impact of specific interference sources, allowing the GNSS receiver to extract precise positioning information from the received signals. These algorithms often leverage advanced signal processing techniques to identify and counteract unwanted components, ensuring the integrity and reliability of GNSS signals. The following is a brief description of the main methods used in the state of the art:

- **Pulse blanking** [37] emerges as a method to combat the impact of pulsed interference. In scenarios where the incoming signal surpasses a predefined power threshold, samples are strategically set to zero. This technique proves effective in reducing the influence of pulsed interferences, ensuring a more accurate reception of GNSS signals. Given its application in safety-critical domains such as civilian aviation, pulse blanking stands out as a valuable tool for real-time interference mitigation. Furthermore, this technique can be extended to the frequency domain and is particularly useful for low bandwidth tone and chirp mitigation.

- **Adaptive notch filter** [38] is a dynamic method employed in the time domain to counteract the influence of interference. By continuously estimating the instantaneous frequency of the jamming signal and filtering out the corresponding frequency from the incoming signal, this method excels in scenarios where interference characteristics evolve rapidly. Its real-time adaptability makes it well-suited for mitigating dynamic interference sources, enhancing GNSS signal fidelity in applications like intelligent transportation systems.

- **Discrete Fourier transform (DFT)** projects a signal into frequency domain. By transforming the signal into the frequency domain and applying a threshold to identify and eliminate suspicious frequency components, this method provides an effective means to suppress unwanted interference. Its adaptability across various frequency regimes makes it a valuable tool for mitigating interference sources with diverse spectral characteristics.
- **Karhunen-Loeve transform (KLT)** [39, 40] introduces a transformation based on the autocorrelation eigenvalues and vectors of the incoming signal. This method explores the statistical properties of the signal, enabling a sophisticated analysis for interference mitigation. Its application is particularly relevant in scenarios where interference exhibits complex statistical patterns. By leveraging the KLT, the project aims to enhance interference mitigation capabilities and refine GNSS signal reception in challenging environments.
- **Bayesian EM under constant modulus** [41] proposes a methods to mitigate the interference characterized by the constant envelope property. It proposed to uses a maximum likelihood estimator for the relevant parameters (time delay and Doppler shift) while considering the presence of latent variables characterized by the constant modulus property.

2 Implemented Mitigation Techniques

The objective of this section is to describe the methods implemented during this project. Namely:

- The Karhunen-Loeve Transform (KLT).
- The Pulse Blanking (PB).

The choice to test this methods primarily stems from their established reputation as state-of-the-art benchmarks, making them the standard to beat. Nevertheless, these methods have not previously been evaluated against open-sky conditions (classical CRB) and the theory of misspecified estimation, making it challenging to compare their effectiveness in interference mitigation. On,the other hand, "*Bayesian EM under constant modulus*" method offer enhancements to these approaches under specific conditions, such as in the presence of wideband interference. However, recent comparisons of this method against the tools presented above have already been conducted in [41]. Therefore, we have not included the study of this method in the manuscript.

2.1 Karhunen-Loeve Transform

The Karhunen-Loève Transform (KLT) is a signal processing technique that can be employed for interference mitigation in the GNSS context. In comparison to the Fast Fourier Transform (FFT), the KLT offers distinct advantages that are presented in the following table:

	Fast Fourier Transform	Karhunen-Loeve Transform
Decomposition functions	Sines and cosines	Any orthonormal functions
Type of signal analysis 1	Deterministic	Deterministic and stochastic
Optimal frequency range 1	Narrowband signals	Narrowband and Wideband signals
Potential detect feeble signal	Small	High
Complexity	$O(1n * log(n))$	$O(n^2)$

The main difference with respect to the FFT is that KLT can be applied to stochastic process, generating an ideal framework for interference mitigation, since it allows us to differentiate between deterministic signals and random processes such as thermal noise. Let us define the random variable $X(t)$ over the finite time interval $0 \leq t \leq T$, we can describe the $X(t)$ as the following series:

$$\boxed{X(t) = \sum_{n=1}^{\infty} Z_n \Phi_n(t)},$$

with,

- Z_n : Random scalar variables,
- $\Phi_n(t)$: Eigenvectors of X.

Here the given equation looks like the FFT decomposition. However, the main difference is that $X(t)$ is a pure random variable. In [42] Maccone proposed to compute the random variable Z_n as follows:

$$\boxed{Z_n = \int_0^T X(t)\Phi_n(t)dt}$$

In this configuration, we observe that we can encompass the entire signal due to the continuity of the integral. The main advantage of this equation is that it allows us to retrieve information from an interfered signal by examining the variance of the KL expansion coefficient Z_n (these variances correspond to the eigenvalues of $\Phi_n(t)$). In fact, Maccone discovered that a signal consisting solely of pure noise is characterized by KLT eigenvalues uniformly distributed and equal to 1. Therefore, this serves as an indicator of any concealed signal within our main signal if certain eigenvalues exceed one. Then, to obtain the the eigenvalues/eigenvectors of the signal, the KLT method computes the covariance of the random variable as follows:

$$\boxed{\int_0^T E[X(t_1)X(t_2)]\Phi_n(t_1)dt_1 = \lambda_n \Phi_n(t_2)}$$

Note that it represents the auto-correlation of a stochastic process $X(t)$ at instant t_1 and t_2. Thanks to this, we can identify the eigenvalues/eigenvectors related to the non-stochastic content of the signal. Nevertheless, as we are working with sampled signals, we can replace the integral by a sum :

$$\boxed{\sum_{k=1}^{N} E[X_k X_l]\Phi_{nk}\Delta t = \lambda_n \Phi_{nl}}$$

With $E[X_k X_l]$ a Toeplitz auto-correlation matrix of size $N \times N$, which can lead to some complexity issue if N become high. Consequently our main objective for KLT is to marked significantly high eigenvalues as interference eigenvalues and the others as the eigenvalues of the signal. To illustrate this idea, we can illustrate the following graph (To make it clear that this is merely an illustrative example, far from reality.) :

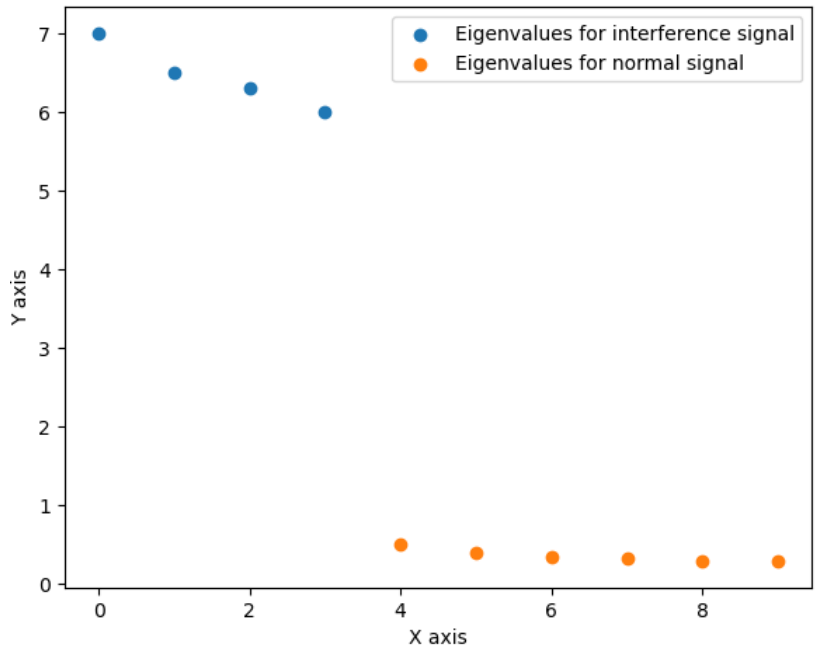

Figure 3: Representation of eigenvalues for a PRN signal vs PRN with interference

For this toy example, it is easy to see a clear separation between eigenvalues, but what about the eigenvalues that do not exhibit this type of pattern, i.e., eigenvalues where it is impossible to clearly distinguish those that reflect an interference signal from those that simply reflect the signal? Also, what happens when we add thermal noise to our signal? Obviously the most difficult thing is to automatize the detection process in order to mitigate the interference as much as possible and to leave the corresponding signal components.

Numerous state-of-the-art methods were examined, yet none yielded conclusive results. Consequently, we opted to conduct an analysis of eigenvalue patterns for instances of signal reception in the presence and absence of interference. For instance, in Figure 5, we depict the eigenvalues for scenarios involving the reception of a 1 ms GPS L1 C/A signal sampled at 4 MHz, both with and without a 20 KHz bandwidth chirp interference. Here, we observe a pattern closely resembling that depicted in Figure 3, suggesting a natural inclination to filter out eigenvalues surpassing the magnitude of the non-interference scenario. However, upon analyzing a different type of interference, such as a higher bandwidth chirp (please refers to Figure 7 for a chirp with $B = 1$MHz), we notice a modification in this pattern. Specifically, interference components are represented by eigenvalues that may fall below

those of the non-interference scenario. To address this issue, a proposed solution involves fixing the threshold not based on eigenvalue magnitude, but rather on its derivative. This is due to the heightened concentration of energy in the interference, causing eigenvalues corresponding to interference to increase non-linearly, thus allowing to find a detection pattern. Note that thank to this method, for the particular case in Figure 7, we can detect until 200 extra eigenvalues corresponding to the interference.

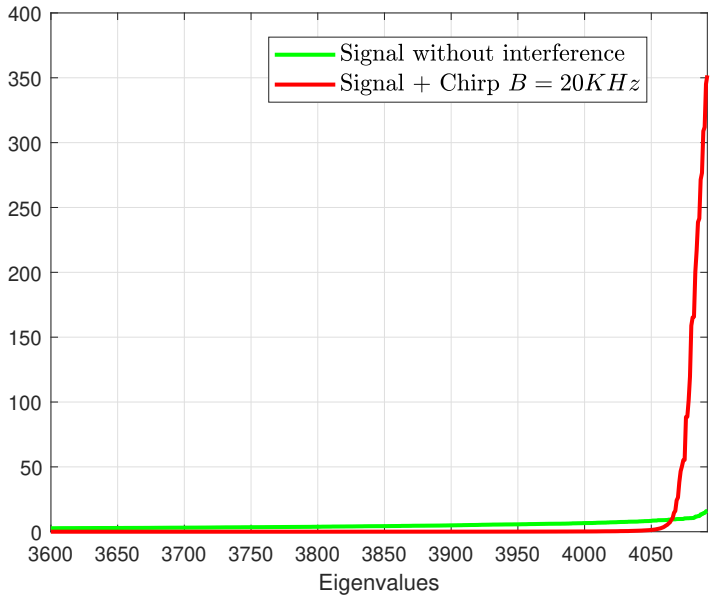

Figure 4: Eigenvalues for the GPS C/A signal at $F_s = 4MHz$ without and with a Chirp Interference with $B = 20KHz$.

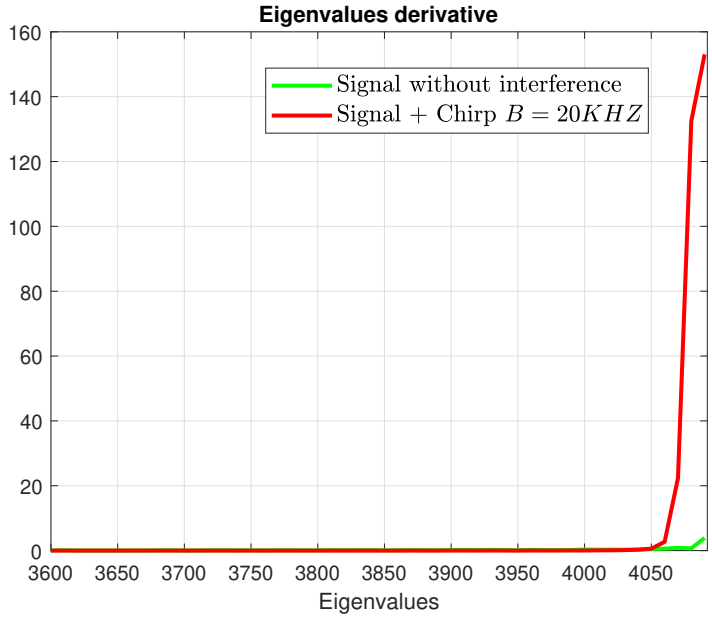

Figure 5: Eigenvalues derivative for the GPS C/A signal at $F_s = 4MHz$ without and with a Chirp Interference with $B = 20KHz$.

After implementing the method, we assess interference mitigation under ideal conditions, meaning without additional noise. This evaluation covers both a single tone

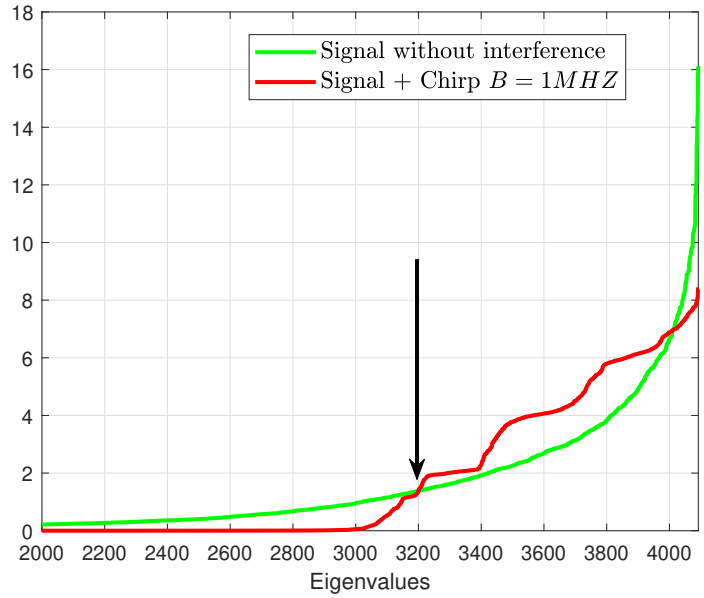

Figure 6: Eigenvalues for the GPS C/A signal at $F_s = 4MHz$ without and with a Chirp Interference with $B = 1MHz$.

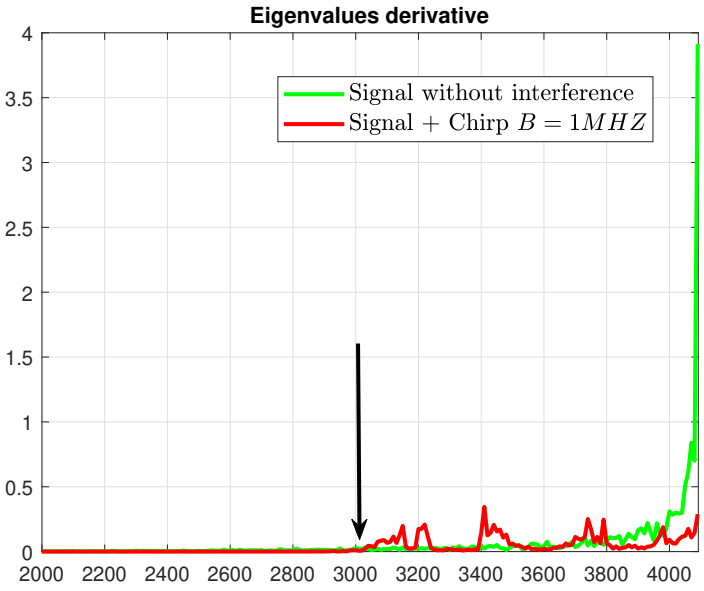

Figure 7: Eigenvalues derivative for the GPS C/A signal at $F_s = 4MHz$ without and with a Chirp Interference with $B = 1MHz$.

scenario (please see Figure 9) and a chirp scenario with a bandwidth of 1 MHz (please refer to Figure 11). In both scenarios, it is be evident that although the recovery may not be flawless, interference has been significantly reduced. Lastly, before discussing the pulse blanking method in detail, it is important to highlight the high complexity of the KLT method. This complexity stems from the necessity of conducting an eigenvector decomposition, a procedure known for its $O(N^3)$ complexity.

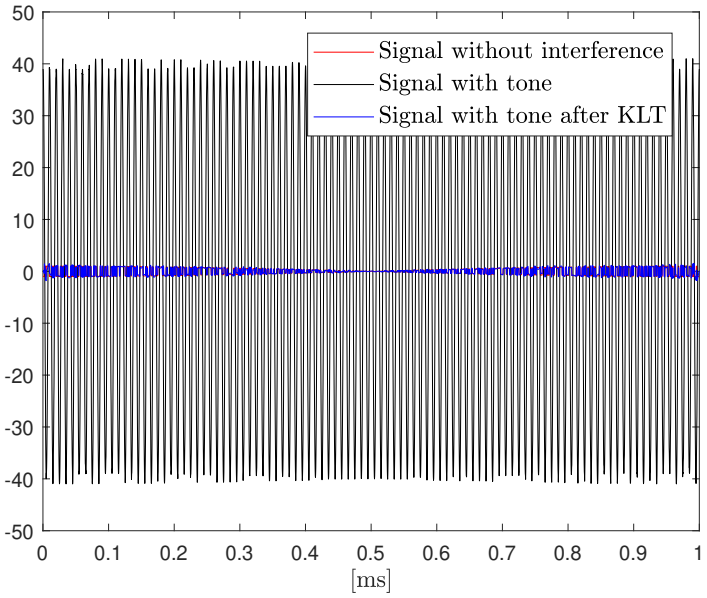

Figure 8: Signal GPS C/A signal at $F_s = 4MHz$ without and with a tone interference. Signal with interference after KLT algorithm.

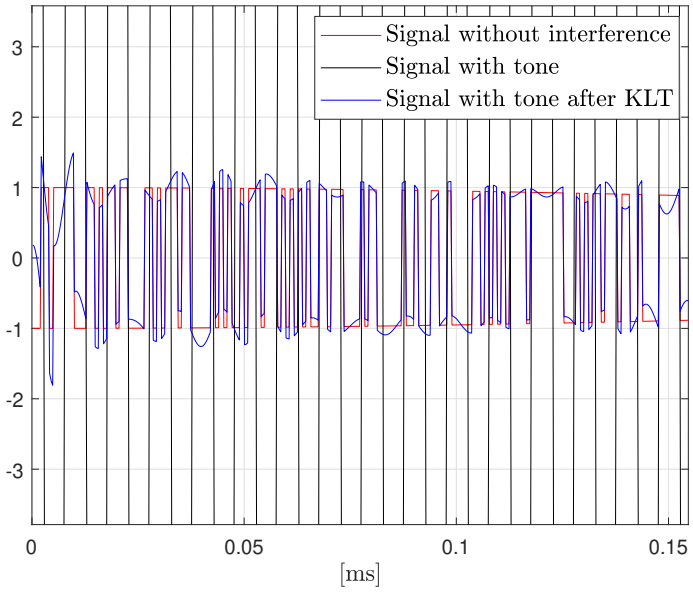

Figure 9: Zoom Signal GPS C/A signal at $F_s = 4MHz$ without and with a tone interference. Signal with interference after KLT algorithm.

2.2 PB : Pulse Blanking

Pulse Blanking (PB) is an effective method for mitigating pulsed interference. The basic principle of PB is illustrated in Figure 12. If the input signal, $y[n]$, has a magnitude greater than a fixed threshold T_h, then the output signal $y_B[n]$ is set to zero. Otherwise, $y_B[n]$ is equal to the input signal, $y[n]$. The filter obtained by applying the PB is usually

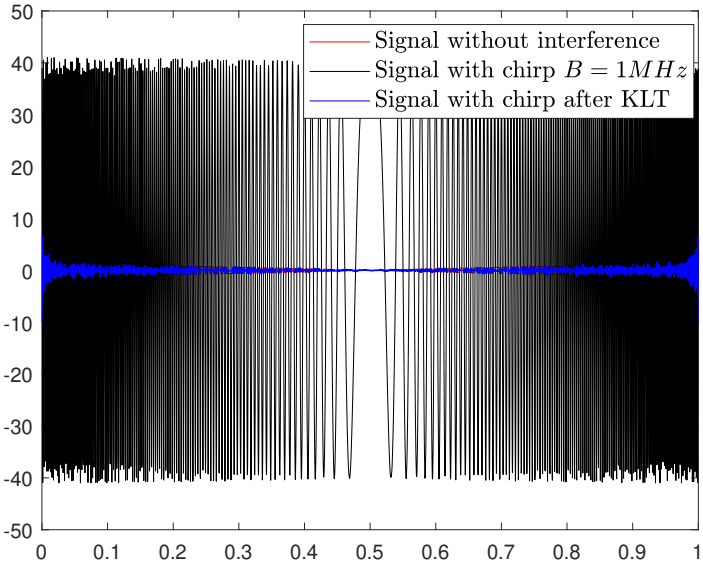

Figure 10: Signal GPS C/A signal at $F_s = 4MHz$ without and with a chirp interference $B = 1MHz$. Signal with interference after KLT algorithm.

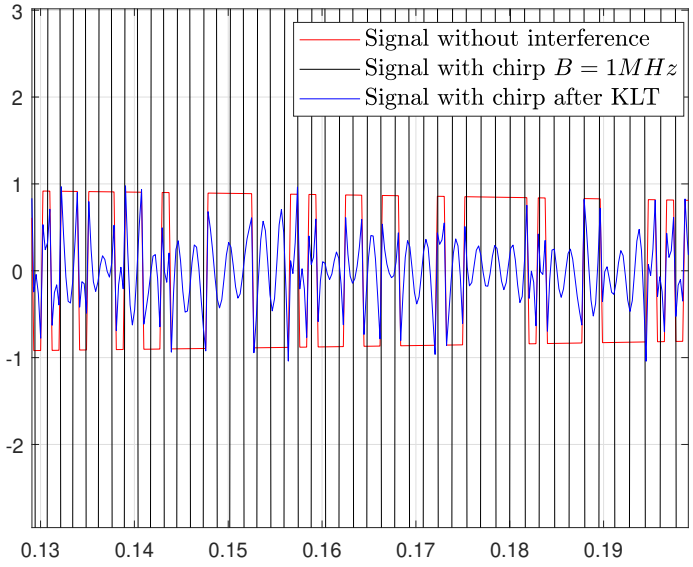

Figure 11: Zoom Signal GPS C/A signal at $F_s = 4MHz$ without and with a chirp interference $B = 1MHz$. Signal with interference after KLT algorithm.

denoted as a pulse blanker and is characterized by the following input-output relationship:

$$y_B[n] = \begin{cases} y_B[n] & \text{if } |y[n]| < T_h \\ 0 & \text{if } |y[n]| \geq T_h \end{cases} \tag{11}$$

The blanking threshold is usually set to guarantee a fixed probability of false alarm, i.e., the probability of blanking samples even if the interference pulse is absent. Thus,

$$P(|y[n]| > T_h \,|\, p[n] = 0) = P_{fa}, \tag{12}$$

where P_{fa} is a target false alarm probability. Under the Gaussian approximation of

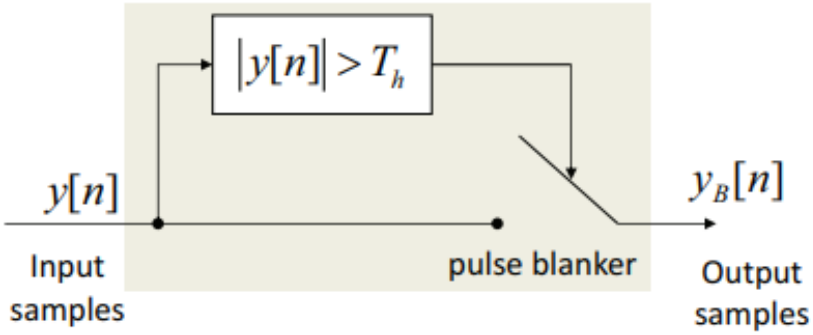

Figure 12: Schematic representation of a pulse blanker [37]

the input signal and considering that the signal is i.i.d, the false alarm probability is given by

$$P(|y[n]|> T_h \,|\, p[n] = 0) = \exp\left(-\frac{T_h^2}{2\sigma^2}\right), \tag{13}$$

yielding to a threshold equals to

$$Th = \sqrt{-2\sigma^2 \log Pt_{fa}} \tag{14}$$

The primary issue with this approach lies in the inability to assume that samples obtained from signal + noise reception are independent and identically distributed (i.i.d) and follow a zero-mean Gaussian distribution. This assumption becomes even less realistic as the signal-to-noise ratio increases, causing the signal magnitude to approach that of the noise. Additionally, having a GNSS signal with an associated Pseudo-Random Noise (PRN) causes the noise to exhibit coloration as soon as the sampling frequency exceeds the signal bandwidth. This undermines the hypothesis test and consequently compromises the accuracy of the theoretical threshold calculation. Once again, similar to the challenge encountered with the KLT, the main obstacle lies in identifying an automated threshold detection method. With this aim in mind, the following approach is proposed in this study: we propose to analyze the histogram of the absolute value of the FFT of the input signal samples produced by the receiver front-end in the absence of interference. Then, we perform the same analyze for the case with interference. Both cases have been illustrated in Figures 13 and 14. Both figures have been made with the same noise power, in this case, a sufficiently high signal ratio.

Based on the patterns depicted in the figures, a potential mitigation approach emerges as follows: establish the threshold at the peak attained in the histogram of the interference-free scenario. Subsequently, in instances where interference is identified, apply frequency filtering—specifically, set to zero all frequency points associated with histogram values surpassing the established threshold. Then, recompute the signal in time from the ifft algorithm. As an example of this method, we assume a chirp interference with a bandwidth equal to 20 KHz. In Figure 15, we illustrate the PSD for the signal without interference, the signal with interference and the signal with interference after applying the PB filter.

In Figure 16, we present a simulated example featuring a chirp interference bandwidth of 1MHz. It is apparent that the primary constraint of this method is that as the interference bandwidth increases, the capability to recover the signal of interest is

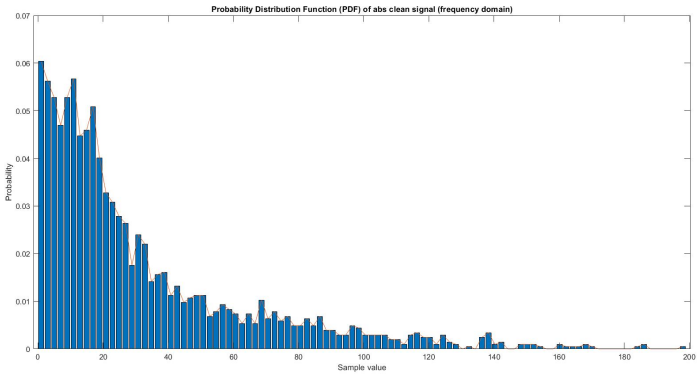

Figure 13: Histogram of the absolute value of the FFT of the signal without interference.

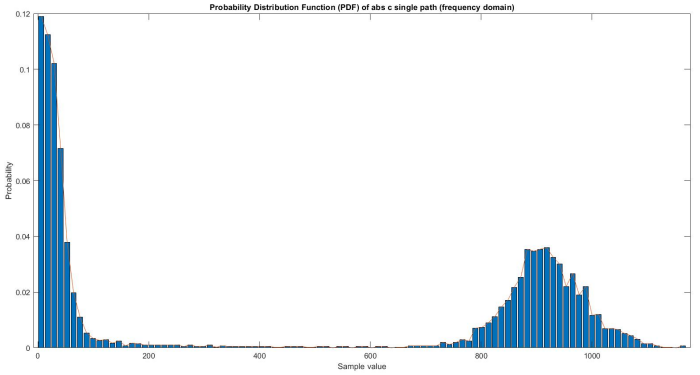

Figure 14: Histogram of the absolute value of the FFT of the signal with interference.

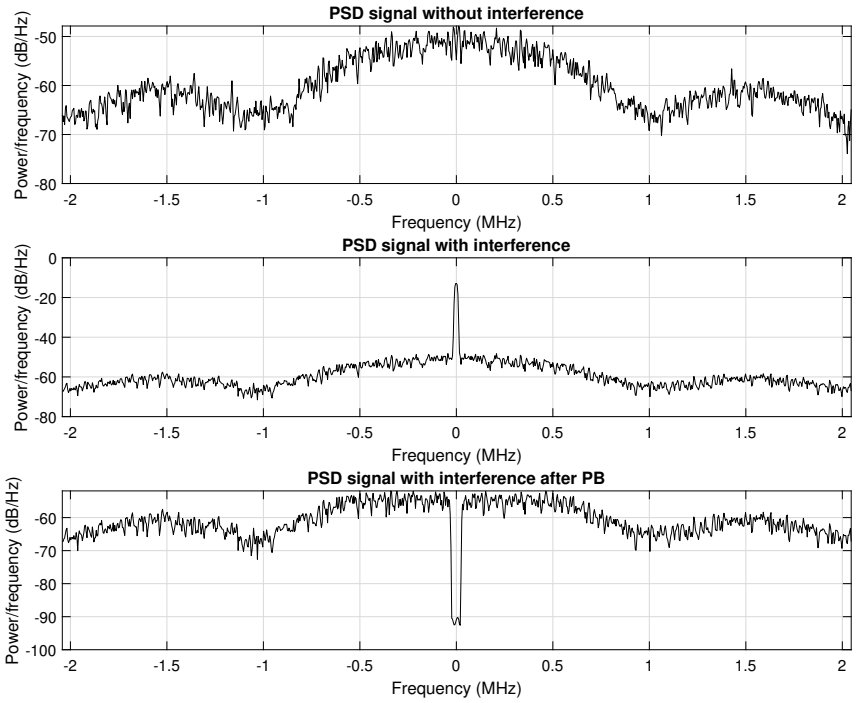

Figure 15: PSD for the signal without interference, the signal with interference and the signal with interference after applying the PB filter.

reduced.

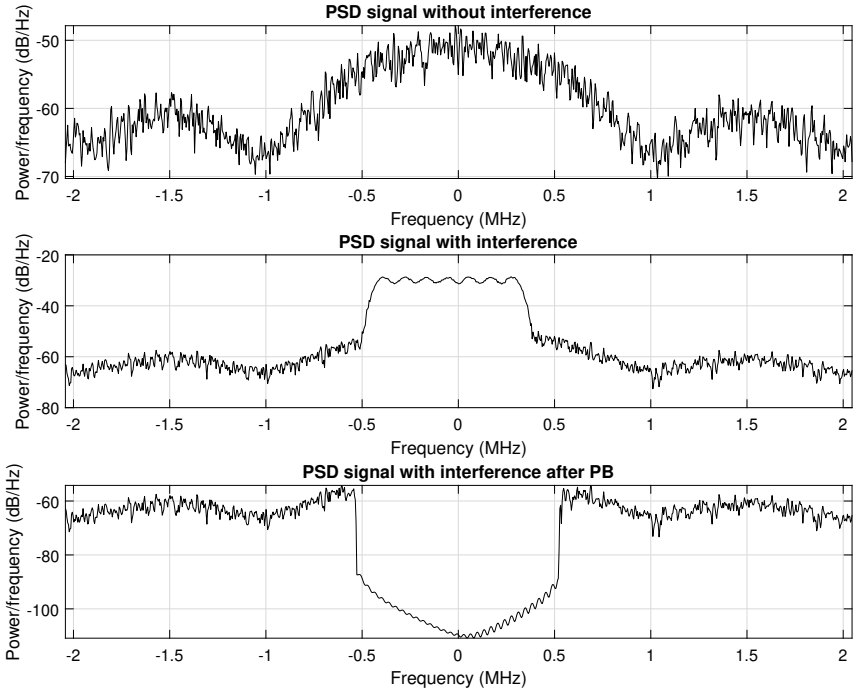

Figure 16: PSD for the signal without interference, the signal with interference and the signal with interference after applying the PB filter.

3 Simulations and Discussion

In order to evaluate the performance of the algorithms presented in Sections 2.1 and 2.2, it is shown several figures depicting the estimation effectiveness in regard to the mean square error of the time-delay and Doppler parameters. These figures include curves illustrating the following metrics:

- the $\sqrt{\text{CRB}}$ (as mentioned in [3]), representing the asymptotic estimation performance of the parameters when no interference is present
- the $\sqrt{\text{MCRB} + \text{Bias}^2}$, depicting the asymptotic estimation performance of the parameters when the receiver is unaware of interference presence (as discussed in [27, 29, 32]). This encompasses the Root Mean Square Error (RMSE) of the misspecified maximum likelihood estimator, as noted in [25]. Please note that these metrics evaluate the RMSE under the assumption that the receiver does not consider any interference, meaning it assumes a misspecified model with a probability distribution differing from the true model. The bias is determined by minimizing the Kullback-Leibler Divergence between the probability distributions of the true model and the assumed model (i.e., the misspecified model).)
- the Root MSE ($\sqrt{\text{MSE}}$) generated by the Misspecified MLE, which converges to the the $\sqrt{\text{MCRB} + \text{Bias}^2}$
- the Root MSE ($\sqrt{\text{MSE}}$) generated by the MLE once the mitigation technique has been applied.

All this metrics are included as a function of the signal to noise ratio at the output of the match filter, denoted as SNR_{out}.

The scenarios we present involve the LFM chirp. This choice is based on the straightforward nature of the tone, making it highly manageable for mitigation and yielding effective results with the algorithms. As for the chirp, we have the flexibility to vary its bandwidths and observe the constraints of the proposed algorithms. We begin by examining scenarios where the interference induces only a minor estimation bias. Subsequently, we move on to situations where the interference entirely disrupts the functionality of the receiver. First of all, let us remember the chirp equation.

$$I(t) = \Pi_T(t) \times e^{j\pi\alpha_c(t-T/2)^2+j\phi},\ \Pi_T(t) = \begin{cases} A_i & \text{for } 0 \leq t < T \\ 0 & \text{otherwise} \end{cases},$$

with α_c the chirp rate, A_i the amplitude and $T = NT_s$ the waveform period. The instantaneous frequency is $f(t) = \frac{1}{2\pi}\frac{d}{dt}(\pi\alpha_c t^2) = \alpha_c t$, and therefore the waveform bandwidth is $B = \alpha_c T$. Due to the computational complexity of the KLT algorithm, it is limited to carry out simulations at a maximum of 1ms. Therefore, we use the GPS L1 C/A signal, with a sampling rate of $F_s = 4$ MHz.

Scenario 1: In a first scenario we assume a chirp with a bandwidth equal to $B = 200$ KHz and an amplitude $A_i = 12.5$, i.e. 11 dB greater than the amplitude of the signal. Then, Figures 17 and 18 illustrate the RMSE for time-delay and Doppler estimation. Each RMSE simulation employs 1000 Monte Carlo runs.

In the figures, it can be observed that the mitigation methods outperform the MMLE. Specifically, they are able to mitigate interference from signal-to-noise ratios much smaller

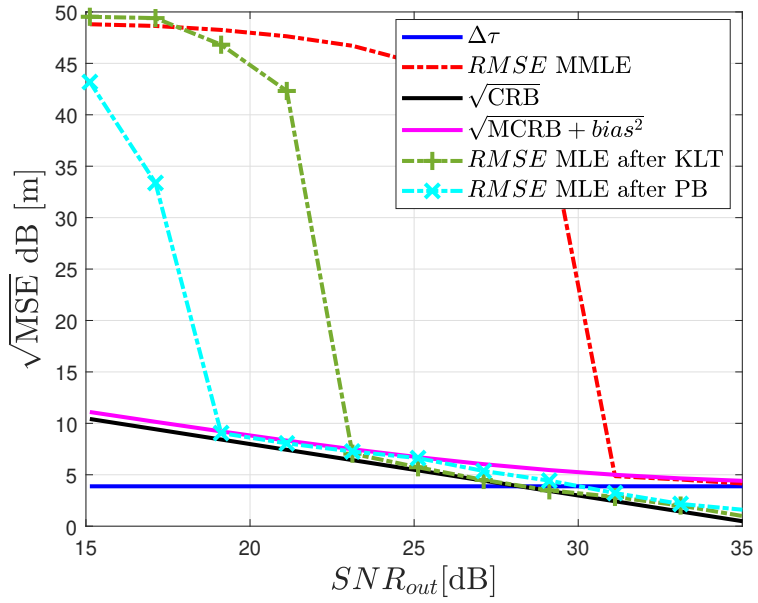

Figure 17: RMSE for time-delay estimation of the GPS L1 C/A signal received along with a centered LFM chirp signal of bandwidth $B = 200$KHz and amplitude $A = 12.5$. The sampling frequency is set to $F_s = 4$ MHz.

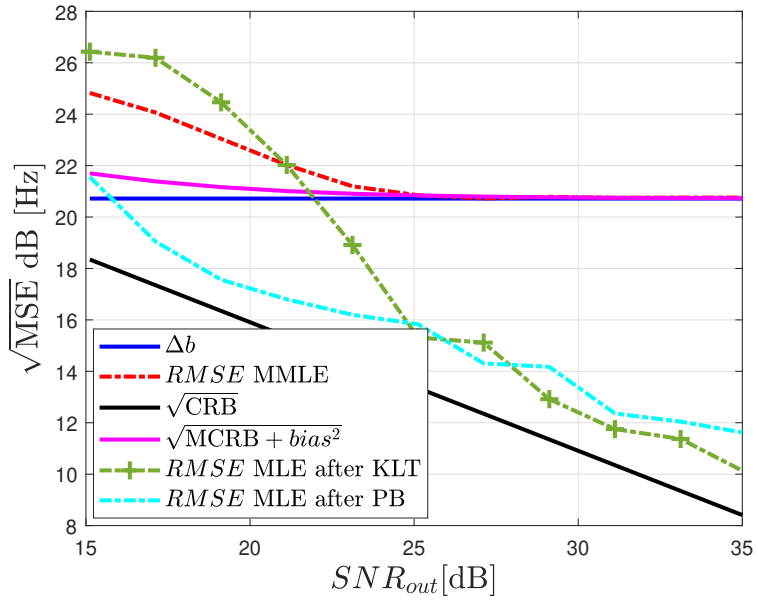

Figure 18: RMSE for Doppler estimation of the GPS L1 C/A signal received along with a centered LFM chirp signal of bandwidth $B = 200$KHz and amplitude $A = 12.5$. The sampling frequency is set to $F_s = 4$ MHz.

than the MMLE's convergence to its asymptotic limit. Additionally, we observe that the methods successfully eliminate the bias generated by the interference. In the case of delay, they are nearly able to achieve the performance of the interference-free scenario, i.e. the limit shown by the CRB. Finally, it should be noted that in this case, the PB method outperforms the KLT as it converges up to 4 dB earlier.

Scenario 2: In a seconds scenario, we assume a chirp with a bandwidth equal to $B = 1$ MHz and an amplitude $A_i = 10$, i.e. 10 dB greater than the amplitude of the signal. Then, Figures 19 and 20 illustrate the RMSE for time-delay and Doppler estimation. Each RMSE simulation employs 1000 Monte Carlo runs.

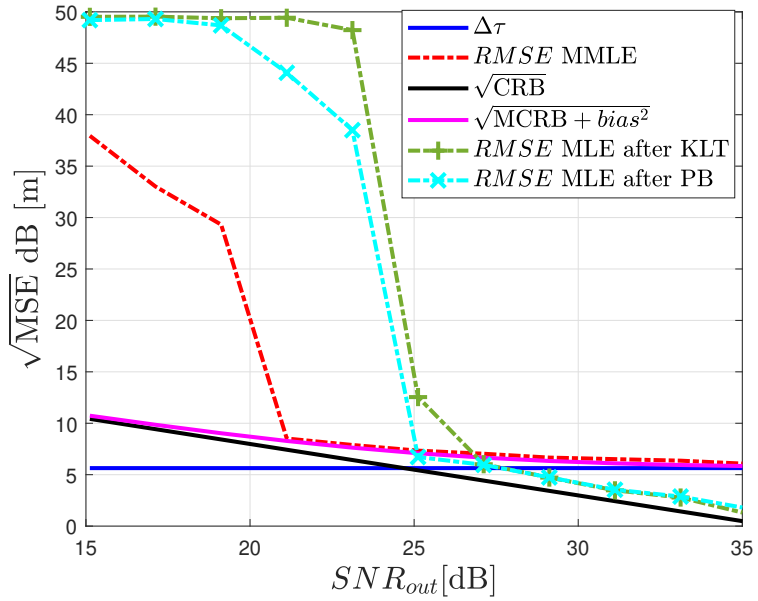

Figure 19: RMSE for time-delay estimation of the GPS L1 C/A signal received along with a centered LFM chirp signal of bandwidth $B = 1$MHz and amplitude $A = 10$. The sampling frequency is set to $F_s = 4$ MHz.

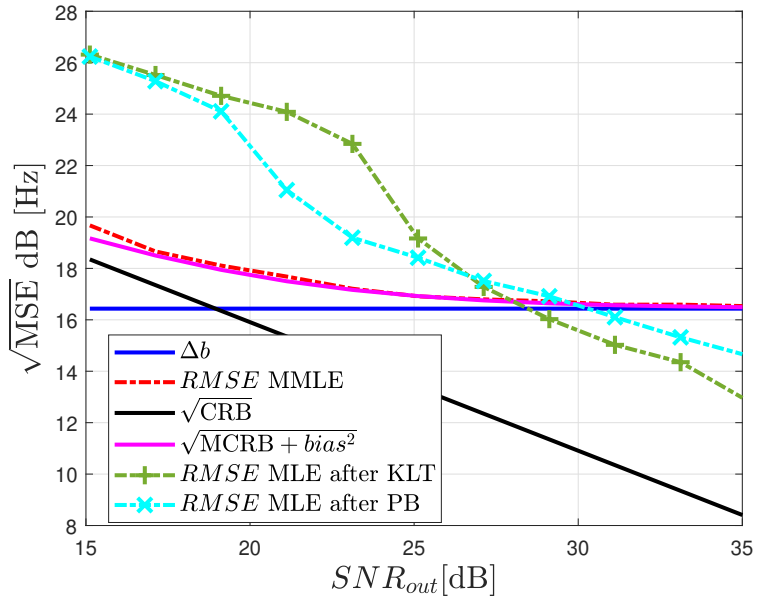

Figure 20: RMSE for Doppler estimation of the GPS L1 C/A signal received along with a centered LFM chirp signal of bandwidth $B = 1$MHz and amplitude $A = 10$. The sampling frequency is set to $F_s = 4$ MHz.

In the Figure 19 and 20, it is evident that the MMLE converges earlier than the mitigation methods. It is observed that increasing the bandwidth of the interference reduces

the effectiveness of the mitigation methods. Specifically, they are able to mitigate interference from much higher signal-to-noise ratios than the convergence of the MMLE to its asymptotic limit. From an SNR_{out} of 25dB, the methods successfully eliminate the bias generated by the interference, and in the case of delay, they nearly achieve the performance of the interference-free scenario. Not much performance difference is observed among the methods for this particular case.

Scenario 3: In a third scenario, we assume a chirp with a bandwidth equal to $B = 2$ MHz and an amplitude $A_i = 40$, i.e. 16 dB greater than the amplitude of the signal. Then, Figures 19 and 20 illustrate the RMSE for time-delay and Doppler estimation. Each RMSE simulation employs 1000 Monte Carlo runs.

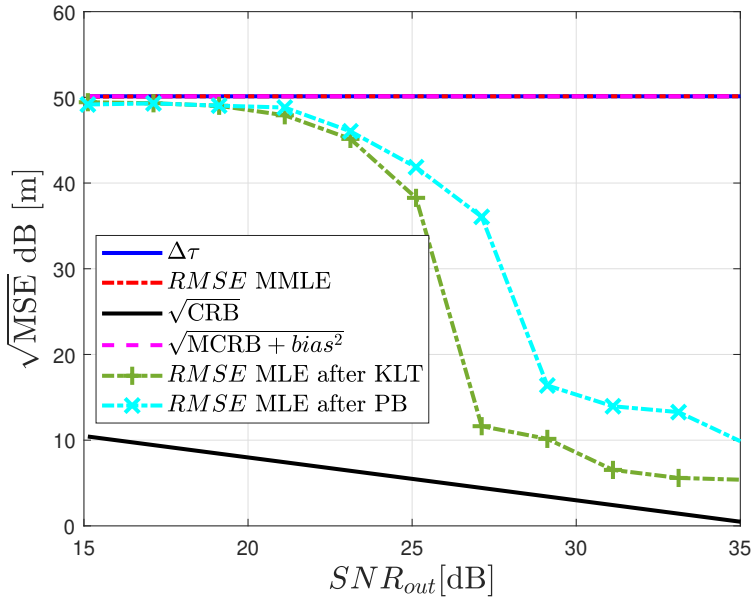

Figure 21: RMSE for time-delay estimation of the GPS L1 C/A signal received along with a centered LFM chirp signal of bandwidth $B = 2$MHz and amplitude $A = 40$. The sampling frequency is set to $F_s = 4$ MHz.

In Figures 21 and 22, it is evident that the MMLE does not work, meaning the receiver is unable to find a coherent solution. However, the mitigation methods can mitigate the effect of interference from a certain SNR_{out} onwards. It should be noted that the KLT method works much better than the PB filter, as the PB filter practically nullifies the entire useful signal component.

Extra Scenario: This scenarios aims to compare the PB with respect to the algorithm proposed in [41]. We assume a chirp with a bandwidth equal to $B = 1$ MHz and an amplitude $A_i = 40$, i.e. 16 dB greater than the amplitude of the signal. Then, Figure 23 illustrates the RMSE for time-delay. Each RMSE simulation employs 1000 Monte Carlo runs.

With this scenario, we aim to demonstrate the superiority of the proposed method in [41] over the classical state-of-the-art methods such as PB. It is observed that the convergence of the proposed method in [41] is at 7 dB.

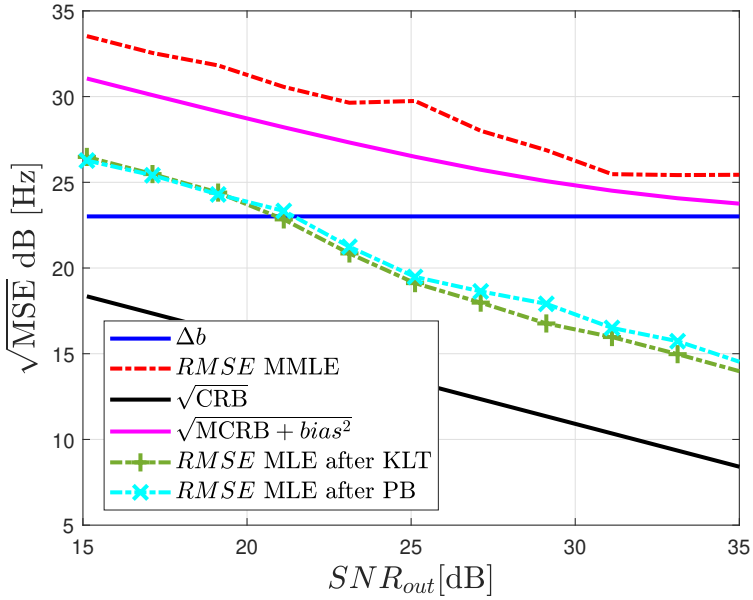

Figure 22: RMSE for Doppler estimation of the GPS L1 C/A signal received along with a centered LFM chirp signal of bandwidth $B = 2$MHz and amplitude $A = 40$. The sampling frequency is set to $F_s = 4$ MHz.

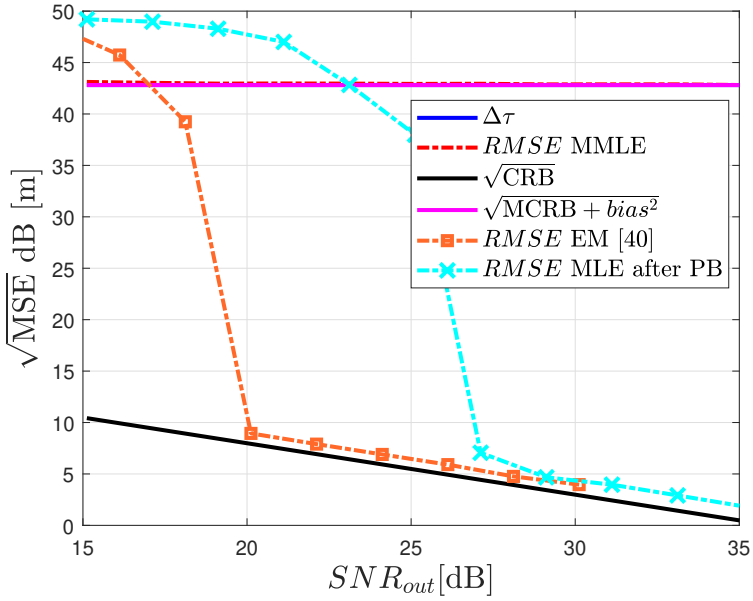

Figure 23: RMSE for time-delay estimation of the GPS L1 C/A signal received along with a centered LFM chirp signal of bandwidth $B = 2$MHz and amplitude $A = 40$. The sampling frequency is set to $F_s = 4$ MHz.

4 Conclusion

In conclusion, existing literature extensively acknowledges the significant impact of interference signals on the performance of GNSS receivers. Various methods in the state of the art have been proposed to mitigate these interferences. However, we have identified a notable gap in the current literature regarding the performance evaluation of these methods using recent tools that enable the computation of GNSS synchronization parameter estimation performance.

The objective of this work has been to address this gap in the state of the art. To achieve this, we have identified the most common interferences and mitigation methods in the literature. We implemented them and calculated their performance using recently proposed estimation tools based on misspecified estimation theory. We have presented several interesting results that allow us to identify the drawbacks of classical methods. Additionally, we have included a comparison with a recent method that has emerged as a potential reference method for mitigating interferences characterized by constant envelope.

References

[1] Petre Stoica and Arye Nehorai. "Performance Study of Conditional and Unconditional Direction of Arrival Estimation". In: *IEEE Trans. Acoust., Speech, Signal Process.* 38.10 (Oct. 1990), pp. 1783–1795.

[2] H. L. Van Trees. *Optimum Array Processing*. Wiley-Interscience, New-York, 2002.

[3] D. Medina et al. "Compact CRB for Delay, Doppler and Phase Estimation - Application to GNSS SPP & RTK Performance Characterisation". In: *IET Radar, Sonar & Navigation* 14.10 (2020), pp. 1537–1549. ISSN: 1751-8792. DOI: 10.1049/iet-rsn.2020.0168.

[4] L. Ortega et al. "Positioning Performance Limits of GNSS Meta-Signals and HOBOC Signals". In: *Sensors* 20.12 (2020), p. 3586. DOI: 10.3390/s20123586.

[5] P. Das et al. "Performance Limits of GNSS Code-Based Precise Positioning: GPS, Galileo & Meta-Signals". In: *Sensors* 20.8 (2020), p. 2196. DOI: 10.3390/s20082196.

[6] L. Ortega, J. Vilà-Valls, and E. Chaumette. "Insights on the Estimation Performance of GNSS-R Coherent and Non-Coherent Processing Schemes". In: *IEEE Geoscience and Remote Sensing Letters* 19 (2022), pp. 1–5. DOI: 10.1109/LGRS.2021.3079579.

[7] L. Ortega, J. Vilà-Valls, and E. Chaumette. "Non-Binary PRN-Chirp Modulation: A New GNSS Fast Acquisition Signal Waveform". In: *IEEE Communications Letters* 26.9 (2022), pp. 2151–2155. DOI: 10.1109/LCOMM.2022.3185319.

[8] C. Lubeigt et al. "Band-Limited Impulse Response Estimation Performance". In: *Signal Processing* 208 (2023), p. 108998. DOI: 10.1016/j.sigpro.2023.108998.

[9] C. Lubeigt et al. "Approximate Maximum Likelihood Time-Delay Estimation for Two Closely Spaced Sources". In: *Signal Processing* 210 (2023), p. 109056. DOI: 10.1016/j.sigpro.2023.109056.

[10] L. Ortega and S. Fortunati. "Misspecified Time-delay and Doppler estimation over non Gaussian scenarios". In: *ICCASP*. Seoul, Korea, Apr. 2024.

[11] S. Fortunati and L. Ortega. "On the efficiency of misspecified Gaussian inference in nonlinear regression: application to time-delay and Doppler estimation". In: *Submitted to: IEEE TSP* ().

[12] Steven M. Kay. *Fundamentals of Statistical Signal Processing: Estimation Theory*. Englewood Cliffs, New Jersey, USA: Prentice-Hall, 1993.

[13] L. Ortega et al. "On the Time-Delay Estimation Performance Limit of New GNSS Acquisition Codes". In: *Proceedings of the International Conference on Localization and GNSS (ICL-GNSS '20)*. Tampere, Finland., 2-4 June 2020. DOI: 10.1109/ITSC45102.2020.9294581.

[14] C. Lubeigt et al. "Joint Delay-Doppler Estimation Performance in a Dual Source Context". In: *Remote Sensing* 12.23 (2020), p. 3894. DOI: 10.3390/rs12233894.

[15] C. Lubeigt et al. "On the Impact and Mitigation of Signal Crosstalk in Ground-Based and Low Altitude Airborne GNSS-R". In: *Remote Sensing* 13.6 (2021). ISSN: 2072-4292. DOI: 10.3390/rs13061085. URL: https://www.mdpi.com/2072-4292/13/6/1085.

[16] H. Mcphee et al. "Accounting for Acceleration – Estimation Performance Limits in High Dynamics Applications". In: *IEEE Transactions on Aerospace and Electronic Systems* 59.1 (2022), pp. 610–622. DOI: 10.1109/TAES.2022.3189611.

[17] J.M Bernabeu et al. "Time-delay and Doppler estimation with a carrier modulated by a band-limited signal". In: *CAMSAP*. Los Sueños, Costa Rica, Dec. 2023. DOI: 10.1109/CAMSAP58249.2023.10403430.

[18] Björn Ottersten et al. "Exact and Large Sample Maximum Likelihood Techniques for Parameter Estimation and Detection in Array Processing". In: *Radar Array Processing*. Ed. by Simon Haykin, John Litva, and Terence J. Shepherd. Heidelberg: Springer-Verlag, 1993. Chap. 4, pp. 99–151.

[19] Ralph O. Schmidt. "Multiple Emitter Location and Signal Parameter Estimation". In: *IEEE Transactions on Antennas and Propagation* 34.3 (1986), pp. 276–280.

[20] Jack Capon. "High-Resolution Frequency-Wavenumber Spectrum Analysis". In: *Proceedings of the IEEE* 57.8 (1969), pp. 1408–1418.

[21] Peter J. Huber. "The Behavior of Maximum Likelihood Estimates Under Nonstandard Conditions". In: *Proc. 5th Berkley Symp. Math. Statist. Probab.* 1967, pp. 221–233.

[22] Hirotugu Akaike. "A New Look at the Statistical Model Identification". In: *IEEE Transactions on Automatic Control* 19.6 (1974), pp. 716–723. DOI: 10.1109/TAC.1974.1100705.

[23] Halbert White. "Maximum Likelihood Estimation of Misspecified Models". In: *Econometrica: Journal of the Econometric Society* (1982), pp. 1–25.

[24] A. Mennad et al. "Slepian-Bangs-type formulas and the related misspecified Cramér-Rao bounds for complex elliptically symmetric distributions". In: *Signal Processing* 142 (2018), pp. 320–329. DOI: 10.1016/j.sigpro.2017.07.029.

[25] S. Fortunati et al. "Performance Bounds for Parameter Estimation under Misspecified Models: Fundamental Findings and Applications". In: *IEEE Signal Process. Mag.* 34.6 (2017), pp. 142–157. DOI: https://doi.org/10.1109/MSP.2017.2738017.

[26] C. Lubeigt et al. "Clean-to-Composite Bound Ratio: A Multipath Criterion for GNSS Signal Design and Analysis". In: *IEEE Transactions on Aerospace and Electronic Systems* 58.6 (2022), pp. 5412–5424. DOI: 10.1109/TAES.2022.3172023.

[27] C. Lubeigt et al. "Untangling First and Second Order Statistics Contributions in Multipath Scenarios". In: *Signal Processing* 205 (2023), p. 108868. ISSN: 0165–1684. DOI: https://doi.org/10.1016/j.sigpro.2022.108868.

[28] C. Lubeigt et al. "Developments for MCRB Computation in Multipath Scenarios". 2022. DOI: 10.13140/RG.2.2.34046.25921.

[29] H. McPhee et al. "On the Accuracy Limits of Misspecified Delay-Doppler Estimation". In: *Signal Processing* 205 (2023), p. 108872. DOI: 10.1016/j.sigpro.2022.108872.

[30] L. Ortega, J. Vilà-Valls, and E. Chaumette. "Theoretical Evaluation of the GNSS Synchronization Performance Degradation under Interferences". In: *ION GNSS+*. Denver, Colorado, USA, 2022. DOI: 10.33012/2022.18564.

[31] L. Ortega et al. "GNSS L5/E5 MaximumLikelihood Synchronization Performance Degradation under DME Interferences". In: *IEEE/ION PLANS*. Monterey, CA, USA, Apr. 2023. DOI: 10.1109/PLANS53410.2023.10140102.

[32] L. Ortega et al. "On GNSS Synchronization Performance Degradation under Interference Scenarios: Bias and Misspecified Cramér-Rao Bounds". In: *NAVIGATION: Journal of the Institute of Navigation* 70.4 (2023). DOI: 10.33012/navi.606.

[33] Peter J.G. Teunissen and Oliver Montenbruck. *Springer Handbook of Global Navigation Satellite Systems*. Switzerland: Springer Cham, 2017.

[34] L. Ortega. "Signal optimization for Galileo evolution". PhD thesis. Institut National Polytechnique de Toulouse-INPT, 2019. DOI: 10.13140/RG.2.2.17872.48649.

[35] C. Lubeigt. "Signal Processing for GNSS Reflectometry". PhD thesis. ISAE-SUPAERO, 2023.

[36] Eric Sénant et al. "Tentative new signals and services in upper L1 and S bands for Galileo evolutions". In: *Proceedings of the 31st International Technical Meeting of the Satellite Division of The Institute of Navigation (ION GNSS+ 2018)*. 2018, pp. 913–942.

[37] Daniele Borio. "Swept GNSS Jamming Mitigation Through Pulse Blanking". In: *Proc. 2016 European Navigation Conference (ENC)*. Helsinki, Finland, Aug. 2016, pp. 1–8. DOI: 10.1109/EURONAV.2016.7530549.

[38] Daniele Borio, Cillian O'Driscoll, and Joaquim Fortuny. "Tracking and Mitigating a Jamming Signal with an Adaptive Notch Filter". In: *InsideGNSS* (Mar. 2014), pp. 67–73.

[39] Arkadiusz Szumski. "Karhunen-Loève Transform as an Instrument to Detect Weak RF Signals". In: *InsideGNSS* (May 2011), pp. 56–64.

[40] Fabio Dovis, Luciano Musumeci, and Jaron Samson. "Performance Comparison of Transformed-Domain Techniques for Pulsed Interference Mitigation". In: *Proc. 25th International Technical Meeting of the Satellite Division of The Institute of Navigation*. Nashville, TN, USA, Sept. 2012, pp. 3530–3541.

[41] J. Lesouple and L. Ortega. "An EM Approach for GNSS Parameters of Interest Estimation Under Constant Modulus Interference". In: *Eusipco*. Helsinki, Finland, Sept. 2023. DOI: 10.23919/EUSIPCO58844.2023.10289775.

[42] Claudio Maccone. "A simple introduction to the KLT and BAM-KLT". In: *Mathematical SETI: Statistics, Signal Processing, Space Missions*. Springer, 2012, pp. 411–448.